



Published in final edited form as:

Nanomedicine. 2015 July ; 11(5): 1163–1167. doi:10.1016/j.nano.2015.02.014.

Effects of singlet oxygen generated by a broad-spectrum viral fusion inhibitor on membrane nanoarchitecture

Axel Hollmann, PhD¹, Sónia Gonçalves, PhD¹, Marcelo T. Augusto, MSc¹, Miguel A. R. B. Castanho, PhD¹, Benhur Lee, PhD², and Nuno C. Santos, PhD¹

Nuno C. Santos: nsantos@fm.ul.pt

¹Instituto de Medicina Molecular, Faculdade de Medicina, Universidade de Lisboa, Av. Prof. Egas Moniz, 1649-028 Lisbon, Portugal.

¹Department of Microbiology, Icahn School of Medicine at Mount Sinai, One Gustave L. Levy Place, #1124, New York, NY 10029, U.S.A.

Abstract

Targeting membranes of enveloped viruses represents an exciting new paradigm to explore on the development of broad-spectrum antivirals. Recently, broad-spectrum small-molecule antiviral drug were described, preventing enveloped virus entry at an intermediate step, after virus binding but before virus–cell fusion. Those compounds, including an oxazolidine-2,4-dithione named JL103 that presented the most promising results, act deleteriously on the virus envelope but not at the cell membrane level. In this work, by using atomic force microscopy (AFM), we aimed at unraveling the effects that JL103 is able to induce in the lipid membrane architecture at the nanoscale. Our results indicate that singlet oxygen produced by JL103 decreases membrane thickness, with and expansion of the area per phospholipid, by attacking the double bonds of unsaturated phospholipids. This membrane reorganization prevents the fusion between enveloped virus and target cell membranes, resulting in viral entry inhibition.

Keywords

Broad-spectrum antiviral; singlet oxygen; AFM; membrane organization

Background

Recently, a family of innovative broad-spectrum small-molecule antiviral drugs was described^{1–3}. These molecules prevent enveloped viruses entry at an intermediate step,

© 2015 Published by Elsevier Inc.

Correspondence to: Nuno C. Santos, nsantos@fm.ul.pt.

Publisher's Disclaimer: This is a PDF file of an unedited manuscript that has been accepted for publication. As a service to our customers we are providing this early version of the manuscript. The manuscript will undergo copyediting, typesetting, and review of the resulting proof before it is published in its final citable form. Please note that during the production process errors may be discovered which could affect the content, and all legal disclaimers that apply to the journal pertain.

The authors have declared that no competing interests exist.

Supporting Information

Supplementary data to this article can be found online.

between virus binding and virus–cell fusion. These compounds act deleteriously on the virus envelope, but not at the cell membrane level. Later, we showed that LJ001^{1,3} and its oxazolidine counterpart (JL103)^{2,4}, all belonging to this new class, act as membrane-targeted photosensitizers. They generate singlet oxygen (¹O₂) in the membrane, changing its biophysical properties and leading to the inhibition of the viral-cell membrane fusion necessary for target cell infection^{4,5}. ¹O₂-mediated lipid oxidation targets the C=C double bonds of unsaturated phospholipid acyl chains, introducing polar hydroperoxide groups in the hydrophobic region of the lipid bilayer⁶. The presence of these oxidized phospholipids results in several membrane properties changes, which negatively impact on its ability to undergo the extreme membrane curvature transitions necessary for virus-cell fusion. These compounds only affect the viral membrane, showing no significant cytotoxicity and not affecting cell–cell fusion^{1,2,4}. This is related to the differences between the biogenic properties of cell plasma membranes and those of static viral membranes. Metabolically active host cells have intrinsic mechanisms to repair the lipid damage induced by reactive oxygen species, while viruses lack this ability to revert membrane alterations.

Methods

POPC (1-palmitoyl-2-oleoyl-*sn*-glycero-3-phosphocholine) and DPPC (1,2-palmitoyl-*sn*-glycero-3-phosphocholine) were from Avanti Polar Lipids (Alabaster, AL, USA). The working buffer used throughout the studies was HEPES 10 mM, pH 7.4, in NaCl 150 mM. JL103 and LJ025 (10 mM) stock solutions were prepared in DMSO. Large and small unilamellar vesicles (LUVs and SUVs, respectively) were prepared by extrusion methods, as described elsewhere^{7,8}. Planar supported lipid bilayers (SLBs) were prepared by SUVs deposition, as previously described⁹. SLBs were then allowed to equilibrate for at least 1 h before measurement.

Atomic force microscopy (AFM) measurements were performed on a JPK Instruments Nanowizard II (Berlin, Germany) mounted on a Zeiss Axiovert 200 inverted microscope (Jena, Germany). Imaging was performed in 10 mM HEPES buffer pH 7.4, in contact mode, using uncoated silicon cantilevers CSC38 from MikroMasch (Tallinn, Estonia), with a tip radius of 10 nm, resonant frequency of approximately 14 kHz and spring constant of 0.05 N/m. Images with a scan size of 5×5 μm² and resolution 512×512 pixels² were obtained with scan rates between 0.6 and 1.0 Hz and set points close to 0.2 V. At least three independent images from three different preparations were obtained for each experimental condition. Height and error signal images were collected and analyzed. After 100 min of imaging, SLBs remained unaltered, without domain fusion or membrane degradation after successive scanings.

Results and Discussion

In previous studies, the antiviral compound oxazolidine-2,4-dithione (JL103) revealed to be the most active against several enveloped viruses, in good agreement with its most efficient production of ¹O₂^{2,5}. Here, by first time, we evaluated the effects of JL103 on SLBs, using AFM to assess the morphological changes induced in membrane structure and organization.

For the sake of comparison, LJ025, an inactive analogue of JL103^{1, 2} was also included in this study (Figure 1a).

AFM was used to evaluate the effects of JL103 after 20 min incubation at 100 μ M final concentration on SLBs of POPC:DPPC 1:1 molar ratio. This lipid mixture was selected because it forms a stable and well defined liquid disordered-gel (l_d - s_o) membrane phase coexistence^{10, 11}. In this context, a binary mixture of phospholipid with a double bond at C9 in the oleoyl chain (POPC) and a completely saturated phospholipid (DPPC) (Figure 1b) is a simple model to evaluate the effect of the $^1\text{O}_2$ produced by JL103 on membrane nanoarchitecture. As we previously demonstrated, photosensitization of viral membranes requires the presence of unsaturated acyl chains^{2, 4, 5, 12} (as the case of POPC). In contrast with DPPC a saturated lipid, where there are no carbon-carbon double bonds available for $^1\text{O}_2$ attack. Moreover, JL103 has a low affinity for DPPC bilayers, as shown by fluorescence spectroscopy (*vd.*, Supporting Information).

Phosphatidylcholines (such as POPC and DPPC) are the most common phospholipids in several biological membranes, being POPC frequently the most common phosphatidylcholine^{13, 14}. POPC-DPPC membranes are extensively used in the literature as the simplest model to represent the coexistence of two distinctive lipid phases, sensitive to domain alterations in the presence of interacting molecules or upon the change of any other experimental parameter. Furthermore, the presence of a carbon-carbon double bond in one of the POPC fatty acyl chains and its absence in DPPC make this the most suitable lipid mixture to study the oxidation effect in the presence of JL103.

By comparing the AFM topography images obtained prior and after incubation with JL103 (Figure 2 and Figure S2), we observed changes in the edge region of POPC:DPPC l_d - s_o phase limits, as well as the coalescence of smaller DPPC domains (Figure 2). These changes were not observed on control experiments using the negative control LJ025, despite of its insertion in membranes^{1, 2, 5}, or using buffer with an amount of DMSO equivalent to that added to the bilayers in the experiments with JL103 and LJ025, as solvent from their stock solutions (Figure 2),

In order to get an insight on JL103 effects at the level of the bilayer nanoarchitecture, we measured the fraction of the total area corresponding to each type of domain (l_d and s_o). In the control images, there was *ca.* 50% of each one, as expected, as well as for LJ025. Upon incubation with JL103, there was an 8.7 ± 1.5 % increase on POPC (l_d) area (Figure 3a). In order to demonstrate that the changes on lipid bilayer architecture are induced by the $^1\text{O}_2$ produced by JL103, instead of by the simple insertion of this compound in the membrane, we observed that the increase of POPC area is reverted by the addition of 15 mM sodium azide (NaN_3), a well know singlet oxygen trap, yielding values comparable to the previous controls. The increase on the POPC area after incubation with JL103 may be explained by the change on the projected area of POPC after addition of the hydroperoxide group, $-\text{OOH}$, to the double bond of the unsaturated lipid (Figure 4a), leading to a higher area-per-lipid due to the migration of the $-\text{OOH}$ group to the polar plane of the bilayer^{15, 16}.

Representing the membrane as an elastic plate, the enlargement of the POPC area should be concomitant with a reduction on the thickness of the lipid bilayer. A typical height profile for the samples with lipid phase coexistence is given in Figure 3b, where the height (or thickness) difference between the liquid disordered and gel phases was found to be 0.95 ± 0.03 nm, in good agreement with previous publications^{9, 17}. From the few defects (holes) found in the lipid bilayer, we calculated the full thickness of the bilayer to be ≈ 4.5 nm (Figure 3b). When the thickness difference (ΔZ) was evaluated after 20 min of incubation with JL103, we found a 0.85 ± 0.16 nm increase on this difference (Figure 3c). Controls with buffer, buffer plus DMSO or the inactive compound LJ025 had no significant changes on ΔZ . The same absence of variation was found using JL103 with 15 mM NaN_3 (Figure 3c), confirming that JL103 effects must be associated with $^1\text{O}_2$ production.

It should be noticed that changes on ΔZ are associated to the expansion of POPC area, concomitant with a decrease of POPC thickness or an increase of DPPC thickness forced by the expansion of POPC. However, the expected change on the thickness by the compression-expansion of the domains seems not to be enough to explain the considerable change observed. In this context, other phenomena could be expected to be involved. Namely, the oxidative process carried out by $^1\text{O}_2$ attack may induce the interdigitation of oxidized phospholipids of opposing monolayers (Figure 4b). As previously reported for other oxidized lipid^{18, 19}, this partial interdigitation of the terminal section of the oxidized acyl chains could be induced due to the change on their spatial disposition promoted by the polar groups in the acyl core, leading to a partial displacement toward the polar plane of the bilayer.

In terms of antiviral activity, it is well-known that the physical state of the lipid bilayer has a major influence on several membrane functions, including its ability to adopt different curvatures during the fusion process^{12, 20}. Here, by the first time, we demonstrated at the nanoscopic level that JL103 is able to remodel membrane nanoarchitecture by an oxidative process. Thus, in this lipid reorganization process induced by JL103, the viral membrane may lose its ability to undergo the extreme membrane curvature transitions necessary for the fusion pore formation during the fusion between viral and cell membranes, resulting in viral entry inhibition.

It should be noticed that this is the first study demonstrating, at the nanoscopic level, that the mode of action of this type of viral inhibitors involves an alteration of the membrane organization, and that this alteration is not associated to the presence of the inhibitor by itself, but to the reactive oxygen species produced by it (as demonstrated by the experiments in the presence of NaN_3). Additionally, we were able to demonstrate that these changes on the membrane nanoarchitecture occur due to the oxidation of the double bond of an unsaturated lipid, by singlet oxygen (previously associated to antiviral activity). We believe these new findings offer a rational and a novel assessment strategy for drug development approaches to develop new broad-spectrum fusion inhibitors against enveloped viruses, with improved activity. Finally, it should be highlighted that this is the first time that the effects of this family of broad-spectrum antiviral molecules is studied by AFM.

Supplementary Material

Refer to Web version on PubMed Central for supplementary material.

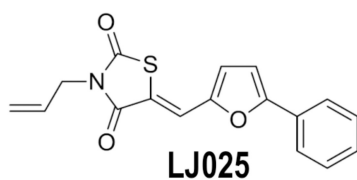
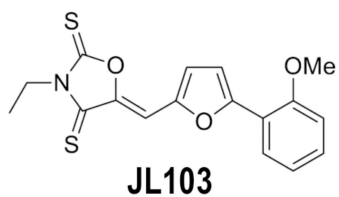
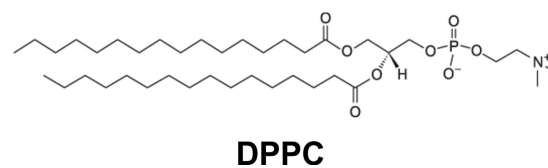
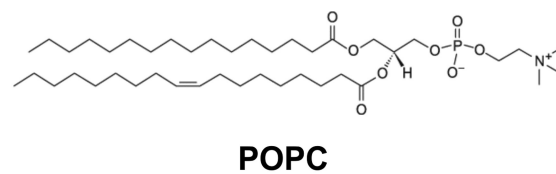
Acknowledgments

Sources of support for research: Fundação para a Ciência e Tecnologia – Ministério da Educação e Ciência (FCT-MEC, Portugal) project VIH/SAU/0047/2011, and fellowships SFRH/BPD/72037/2010 and SFRH/BD/95624/2013 to AH and MTA, respectively. NIH grants U01 AI070495 and U01 AI082100. JL103 and LJ025 were generously provided by Michael E. Jung and Jihye Lee (University of California, Los Angeles).

References

1. Wolf MC, Freiberg AN, Zhang T, Akyol-Ataman Z, Grock A, Hong PW, et al. A broad-spectrum antiviral targeting entry of enveloped viruses. *Proc Natl Acad Sci U S A*. 2010; 107:3157–3162. [PubMed: 20133606]
2. Vigant F, Lee J, Hollmann A, Tanner LB, Ataman ZA, Yun T, et al. A Mechanistic Paradigm for Broad-Spectrum Antivirals that Target Virus-Cell Fusion. *Plos Pathogens*. 2013; 9
3. St Vincent MR, Colpitts CC, Ustinov AV, Muqadas M, Joyce MA, Barsby NL, et al. Rigid amphipathic fusion inhibitors, small molecule antiviral compounds against enveloped viruses. *Proc Natl Acad Sci U S A*. 2010; 107:17339–17344. [PubMed: 20823220]
4. Vigant F, Hollmann A, Lee J, Santos NC, Jung ME, Lee B. The rigid amphipathic fusion inhibitor dUY11 acts through photosensitization of viruses. *J Virol*. 2014; 88:1849–1853. [PubMed: 24284320]
5. Hollmann A, Castanho MARB, Lee B, Santos NC. Singlet oxygen effects on lipid membranes: implication on broad range viral fusion inhibitors mechanism of action. *Biochem J*. 2014; 459:161–170. [PubMed: 24456301]
6. Watabe N, Ishida Y, Ochiai A, Tokuoka Y, Kawashima N. Oxidation decomposition of unsaturated fatty acids by singlet oxygen in phospholipid bilayer membranes. *J Oleo Sci*. 2007; 56:73–80. [PubMed: 17898466]
7. Mayer LD, Hope MJ, Cullis PR. Vesicles of variable sizes produced by a rapid extrusion procedure. *Biochim Biophys Acta*. 1986; 858:161–168. [PubMed: 3707960]
8. Szoka F, Olson F, Heath T, Vail W, Mayhew E, Papahadjopoulos D. Preparation of unilamellar liposomes of intermediate size (0.1–0.2 μmol) by a combination of reverse phase evaporation and extrusion through polycarbonate membranes. *Biochim Biophys Acta*. 1980; 601:559–571. [PubMed: 6251878]
9. Franquelim HG, Gaspar D, Veiga AS, Santos NC, Castanho MARB. Decoding distinct membrane interactions of HIV-1 fusion inhibitors using a combined atomic force and fluorescence microscopy approach. *Biochim Biophys Acta*. 2013; 1828:1777–1785. [PubMed: 23500616]
10. Giocondi M-C, Vié V, Lesniewska E, Milhiet P-E, Zinke-Allmang M, Le Grimellec C. Phase Topology and Growth of Single Domains in Lipid Bilayers. *Langmuir*. 2001; 17:1653–1659.
11. Zhao J, Wu J, Heberle FA, Mills TT, Klawitter P, Huang G, et al. Phase studies of model biomembranes: complex behavior of DSPC/DOPC/cholesterol. *Biochim Biophys Acta*. 2007; 1768:2764–2776. [PubMed: 17825247]
12. Stachowiak JC, Brodsky FM, Miller EA. A cost-benefit analysis of the physical mechanisms of membrane curvature. *Nat Cell Biol*. 2013; 15:1019–1027. [PubMed: 23999615]
13. Lorizate M, Sachsenheimer T, Glass B, Habermann A, Gerl MJ, Krausslich HG, et al. Comparative lipidomics analysis of HIV-1 particles and their producer cell membrane in different cell lines. *Cell Microbiol*. 2013; 15:292–304. [PubMed: 23279151]
14. Brugger B, Glass B, Haberkant P, Leibrecht I, Wieland FT, Krausslich HG. The HIV lipidome: a raft with an unusual composition. *Proc Natl Acad Sci U S A*. 2006; 103:2641–2646. [PubMed: 16481622]

15. Riske KA, Sudbrack TP, Archilha NL, Uchoa AF, Schroder AP, Marques CM, et al. Giant vesicles under oxidative stress induced by a membrane-anchored photosensitizer. *Biophys J.* 2009; 97:1362–1370. [PubMed: 19720024]
16. Weber G, Charitat T, Baptista MS, Uchoa AF, Pavani C, Junqueira HC, et al. Lipid oxidation induces structural changes in biomimetic membranes. *Soft Matter.* 2014; 10:4241–4247. [PubMed: 24871383]
17. Franquelim HG, Loura LM, Santos NC, Castanho MARB. Sifuvirtide screens rigid membrane surfaces. establishment of a correlation between efficacy and membrane domain selectivity among HIV fusion inhibitor peptides. *J Am Chem Soc.* 2008; 130:6215–6223. [PubMed: 18410103]
18. Tirosh O, Kohen R, Katzhendler J, Alon A, Barenholz Y. Oxidative stress effect on the integrity of lipid bilayers is modulated by cholesterol level of bilayers. *Chem Phys Lipids.* 1997; 87:17–22. [PubMed: 9219345]
19. Mason RP, Walter MF, Mason PE. Effect of oxidative stress on membrane structure: small-angle X-ray diffraction analysis. *Free Radic Biol Med.* 1997; 23:419–425. [PubMed: 9214578]
20. Chernomordik LV, Kozlov MM. Protein-lipid interplay in fusion and fission of biological membranes. *Annu Rev Biochem.* 2003; 72:175–207. [PubMed: 14527322]

A**B****Figure 1.**

a) Molecular structures of JL103 and its inactive analogue LJ025^{1,2}. **b)** Molecular structures of the phospholipids POPC and DPPC.

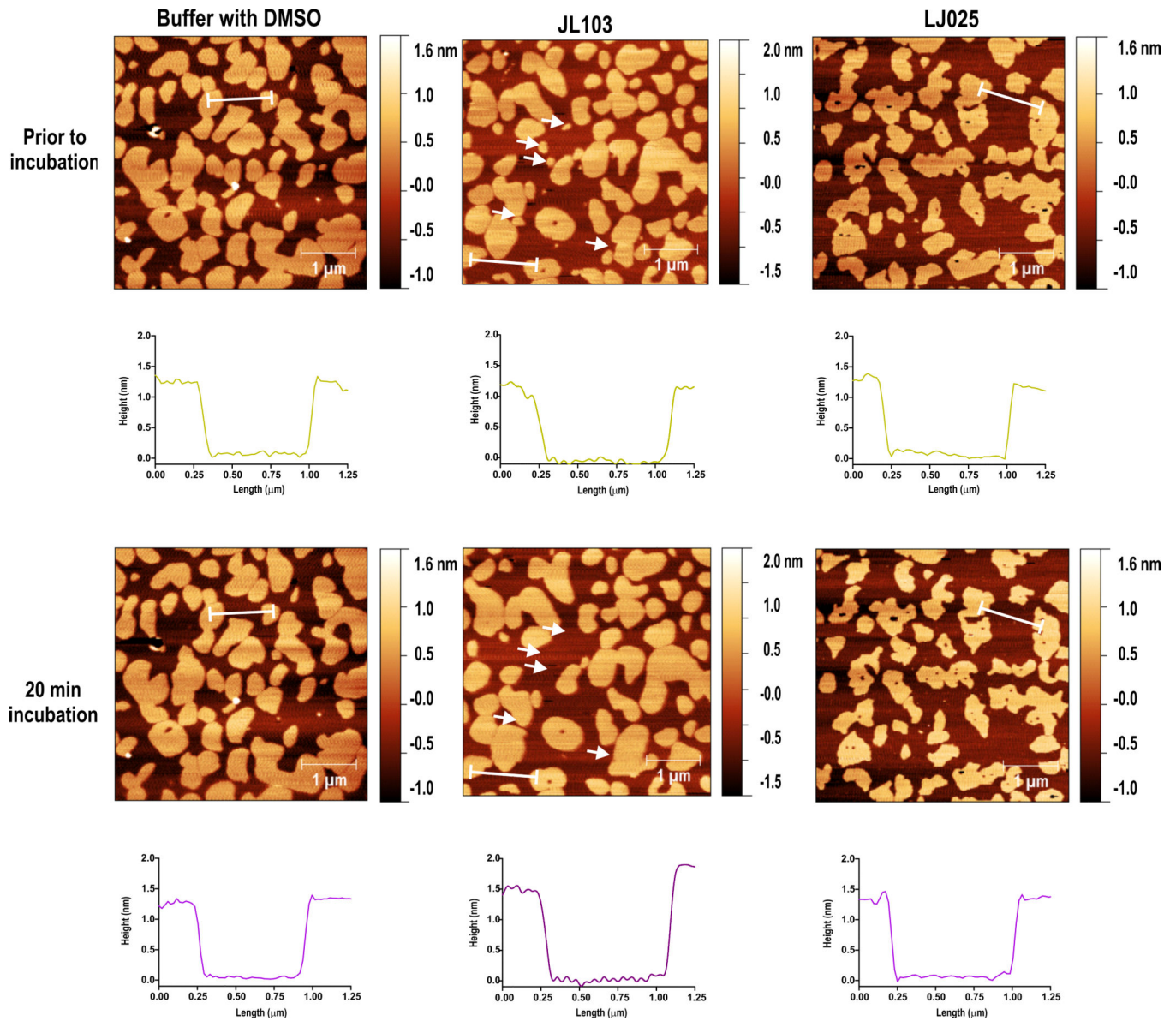


Figure 2.

AFM height images and cross-sections of POPC:DPPC 1:1 bilayers, in HEPES buffer pH 7.4, prior (upper panels) and after 20 min incubation with buffer with DMSO, 100 μ M JL103, or 100 μ M LJ025 (lower panels). Arrows in the JL103 incubation AFM image highlight the coalescence or fading of DPPC domains.

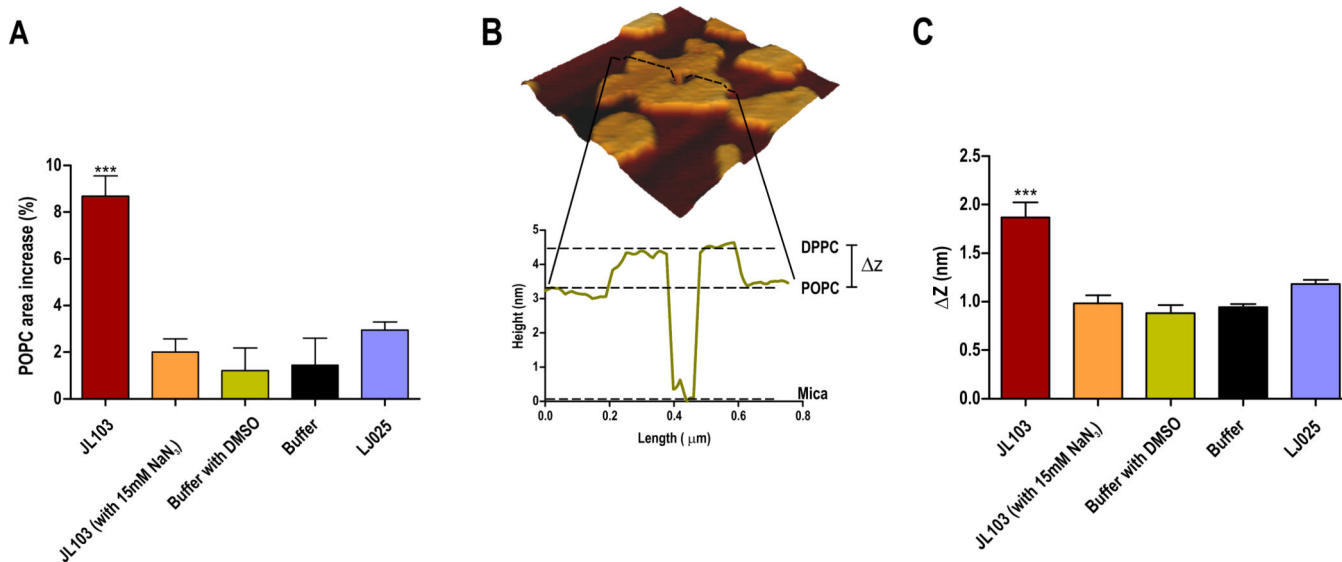


Figure 3.

a) POPC area increase after 20 min incubation with JL103 or controls. The percentage of the area occupied by POPC domains were calculated from AFM images using ImageJ software v. 1.47 (US National Institutes of Health). **b)** Differences in height on POPC:DPPC 1:1 supported lipid bilayers in buffer conditions, assessed on AFM height images. **c)** Differential thickness (ΔZ) of POPC:DPPC 1:1 SLBs after 20 min incubation with JL103 or controls. Data shown are the average of several images from at least two different batches. ***: $p < 0.001$ upon comparison with all other conditions (one-way ANOVA followed by a Bonferroni multiple comparison test).

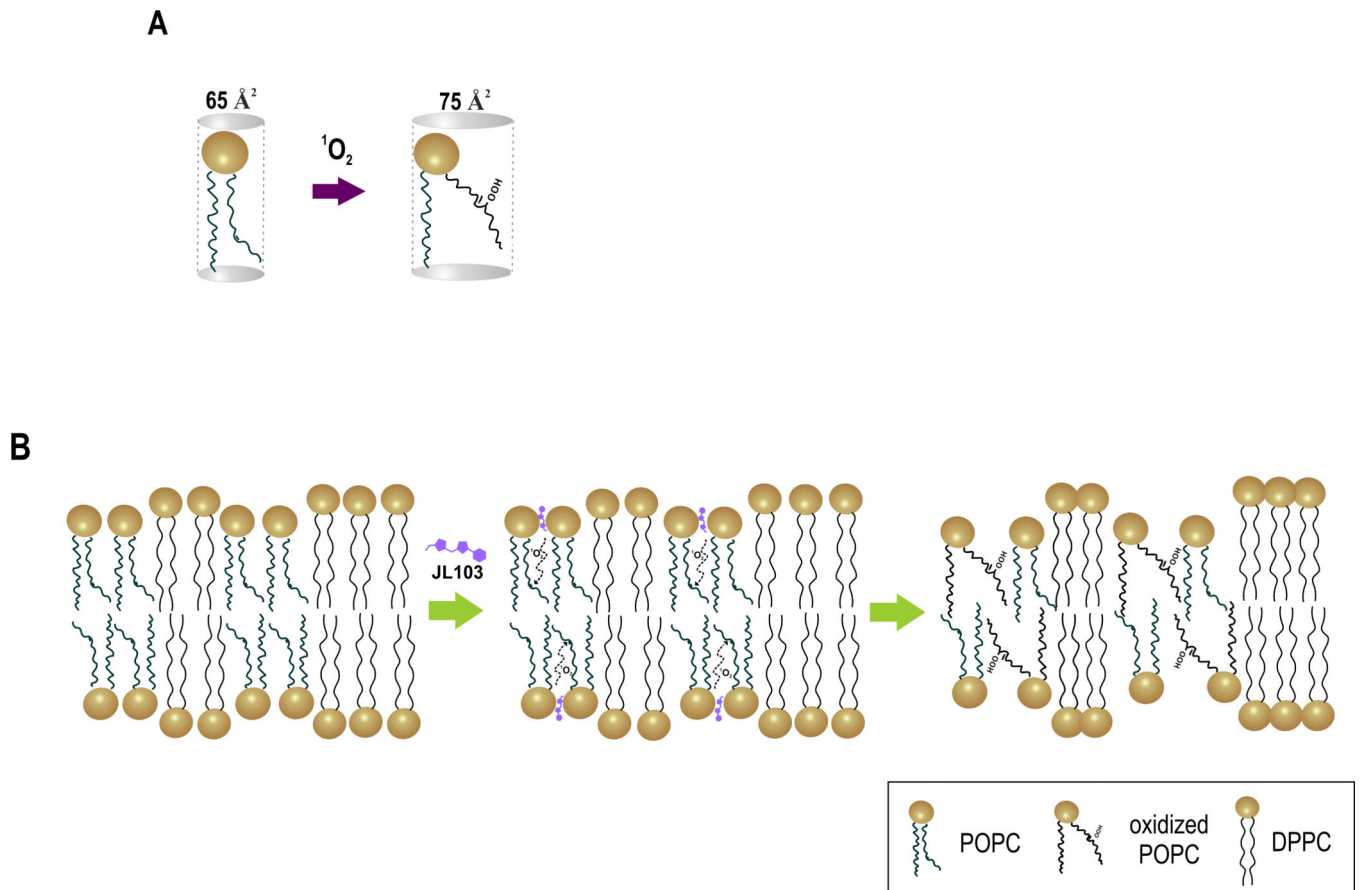


Figure 4.

a) Schematic representation of the area per molecule change on POPC after $^1\text{O}_2$ attack to carbon-carbon double bond (adapted from ¹⁵). **b)** Proposed model of induced re-organization of the membrane phospholipids after being oxidized by the $^1\text{O}_2$ produced by JL103.